Pergamon

Calphad, Vol. 25, No. 2, pp. 217–230, 2001
© 2001 Elsevier Science Ltd
All rights reserved
0364-5916/01/$ - see front matter

PII: S0364-5916(01)00044-X

Simulating the Ferrite-to-Austenite Transformation in Stainless Steel Welds

J. M. Vitek[1]*, E. Kozeschnik[2] and S. A. David[1]
[1] Oak Ridge National Laboratory, ORNL, Bldg: 4508, MS 6096, Oak Ridge, TN 37831
[2] Graz University of Technology
* Corresponding author's e-mail: vitekjm@ornl.gov

(Received June 5, 2001)

Abstract. Under some conditions, the transformation of as-solidified ferrite to austenite in stainless steels has characteristics of a massive transformation. Calculations were carried out to determine if experimental evidence from Koseki of such a transformation could be modeled by a diffusion-controlled transformation. Two different conditions at the transformation interface were considered: ortho-equilibrium and para-equilibrium. Simulations solved the multi-component diffusion problem for various thermal conditions, including isothermal and continuous cooling conditions. It was found that neither interface condition could explain the experimental results of Koseki. The ortho-equilibrium interface condition resulted in transformation rates that were too slow. In addition, continuous cooling conditions led to non-uniform compositions, contradicting the experimental evidence. The para-equilibrium condition resulted in sufficiently fast transformation rates but the temperature of the transformation was considerably higher than that found experimentally. It is suggested that a condition of limited partitioning of substitutional solute elements at the interface could better explain the experimental results, but implementation of this condition at the interface is not possible with currently available simulation capabilities.

Introduction

Stainless steel weld microstructures can be fully austenitic, fully ferritic, or some combination of the two. The final as-welded microstructure at room temperature is determined by the solidification mode and the extent of any solid state transformations (typically ferrite to austenite) during subsequent cooling. In common stainless steel weld metals such as types 304, 308, 309 and 316, a primary ferrite mode of solidification is observed when welding under typical conditions. Some austenite may form in the latter stages of solidification, but most of the austenite forms during solid state transformation of ferrite to austenite during cooling. This transformation is usually incomplete, leaving the final microstructure with residual ferrite, typically on the order of 5 to 15 volume %.

It has been well-documented that under more rapid solidification and cooling conditions, as found during laser or electron-beam welding, the solidification mode may change from primary ferrite to primary austenite for

many austenitic stainless steel weld compositions [1-5]. The competition between ferritic and austenitic growth has been the subject of several investigations [6-10]. Thus, a wide range of microstructures can be found in these materials, depending upon the solidification conditions and the extent of any solid state transformations.

It has been suggested by several authors that under some conditions, a massive transformation of ferrite to austenite can take place during cooling after solidification [4, 11-13]. The microstructures that have led to this conclusion are characterized by an absence of any solidification substructure, such as dendrites, and a uniform austenite composition with no sign of microsegregation. There has been some debate as to the origin of fully austenitic weld microstructures that show no solidification substructure and are free of any microsegregation. In addition to the massive ferrite-to-austenite transformation interpretation, such microstructures can be the product of planar growth solidification of austenite. As noted before, non-equilibrium austenitic solidification has been found often under rapid cooling conditions [1-5]. Under such rapid cooling conditions, planar growth with minimal solute partitioning, or even the total absence of partitioning, during solidification is plausible. Unfortunately, investigation of as-solidified microstructures is complicated by the potential for solid state transformation during subsequent cooling to room temperature. Hence, experimental evidence is often insufficient to distinguish between these two alternatives.

It is the purpose of this study to simulate the ferrite-to-austenite transformation and to determine if the experimental results can be explained by a diffusion-controlled transformation mechanism. Two different simulations were undertaken. In both, the transformation was assumed to be controlled by long-range diffusion driven by either one of two local equilibrium conditions at the ferrite-austenite interface. In the first case, it was assumed that ortho-equilibrium between the ferrite and austenite was maintained at the moving interface and, consequently, substitutional solute diffusion controlled the rate of the transformation. In the second case, para-equilibrium was imposed at the ferrite-austenite interface and the formation of austenite was controlled only by the rapid diffusion of interstitial carbon. The results of the simulations are compared to the experimental data and conclusions as to the mechanisms that control the ferrite to austenite transformation are drawn. The present investigation focused on the experimental work of Koseki [9, 13], in which evidence was provided that clearly indicated that the final austenite was the product of a solid state transformation.

Experimental Data for Ferrite to Austenite Transformation

Koseki examined the solidification microstructure in levitation-melted droplets of a nominal ternary Fe-18.51 Cr-11.34 Ni (wt %) alloy that was undercooled by over 100 K prior to solidification. Thermal measurements of the droplet surface during cooling showed two recalescence peaks during cooling, as shown in Fig 1a. The corresponding micrographs showed large austenite grains at the surface, as shown in Fig 1b. The second recalescence peak was found after solidification was complete and was indicative of a solid state transformation. Furthermore, Koseki analyzed the composition distribution in samples quenched before the second recalescence reaction and found evidence of microsegregation characteristic of primary ferrite formation, i.e., noticeable nickel partitioning and minimal chromium microsegregation [14]. These two observations lead to the conclusion that the highly undercooled droplets solidified in the primary ferrite mode, with some associated solute partitioning and compositional inhomogeneity. During further cooling, rapid diffusion within the BCC ferrite eliminated the small compositional gradients prior to the solid-state transformation of ferrite to

austenite. The thermal profile in Fig 1a shows a break in the continuous cooling curve (shown by an arrow) and this is taken as the start of the ferrite-to-austenite transformation. Thus, this thermal profile can be used to provide some guidance as to the time and temperature conditions for the solid-state transformation. From the figure, one can conclude that the ferrite-to-austenite transformation takes place within approximately 1/4 s at about 1630 K.

Simulation Procedures

The ferrite-to-austenite transformation was modeled as a diffusion-controlled reaction driven by a local equilibrium constraint at the interface. One-dimensional diffusion was considered. The "diffusion cell" was set initially as 100% ferrite of uniform composition. Only the transformation to austenite was considered; liquid or precipitate formation was not allowed in the simulation. Various cell sizes were considered, but the maximum cell size was set at 100μm, which is roughly equivalent to the half-width of the austenite grains found experimentally (see Fig. 1b).

Several different thermal conditions were examined. Some calculations were performed for isothermal transformation conditions, while others simulated continuous cooling conditions. Various cooling rates up to 100 K/s were considered. The thermal history profile shown in Fig 1a indicates that a steady state cooling rate of about 100 K/s prevailed during most of the cooling from 1650 to 1500 K, interrupted only by the recalescence reaction at ~ 1630 K. The choice of cell size and cooling rate was often limited by the numerical simulation routines.

The transformation simulation under the condition of ortho-equilibrium at the interface[1] was carried out with the Dictra software [15]. The standard mobility database within Dictra was used to describe the atomic mobilities as a function of temperature and composition. The ortho-equilibrium condition at the interface was calculated with the use of the ThermoCalc software [16] and the SSOL database [17].

For the simulation condition of local para-equilibrium at the interface, the MatCalc software was used [18]. The para-equilibrium constraint provides that the occupancies of the substitutional solute atoms in the sublattice model remain constant while only the interstitial carbon concentrations are allowed to vary [19]. Under these conditions, the minimum energy condition results in equal carbon chemical potentials at the interface while the chemical potentials of the solute atoms are not equal, but rather discontinuous, at the interface.

The alloy used by Koseki in his experimental study was a "pure" Fe-Cr-Ni ternary alloy and its composition is shown in Table 1. A small carbon concentration was present. For the simulation studies, only four components were considered (Fe, Cr, Ni, and C) and all other components were ignored. The inclusion of the carbon concentration when carrying out the ortho-equilibrium calculations often led to numerical difficulties in the simulation. Nevertheless, some calculations were carried out for the ortho-equilibrium condition with and

[1] For brevity, the "ortho-equilibrium condition at the interface" will be referred to simply as the "ortho-equilibrium condition", even though this condition only applies at the interface and not throughout the calculation cell. Similarly, the "local para-equilibrium condition at the interface" will be referred to simply as the "para-equilibrium condition".

without carbon for comparable conditions. It was found that the inclusion of carbon in these simulations had basically no effect, other than to make the simulations numerically more difficult. Therefore, for numerical simplicity, the composition used in the ortho-equilibrium condition calculations was restricted to only the ternary Fe-Cr-Ni alloy whereas the quaternary Fe-Cr-Ni-C alloy was considered for the para-equilibrium condition simulations. These compositions are also noted in Table 1.

Table 1: Alloy Composition Used in Calculations (in wt %) [13].

Element	Overall alloy composition	Alloy composition used for ortho-equilibrium simulations	Alloy composition used for para-equilibrium simulations
Cr	18.51	18.51	18.51
Ni	11.34	11.34	11.34
C	0.003	0	0.003
Si	<0.01	0	0
Mn	<0.01	0	0
P	<0.001	0	0
S	<0.001	0	0
N	0.001	0	0
O	0.008	0	0
Fe+Cr+Ni	>99.96	100	99.997

Results

Phase Diagrams

The thermal conditions for the simulations and the interpretation of the results are related to the phase equilibria imposed at the interface. Therefore, for reference, calculated phase diagrams under both ortho- and para-equilibrium conditions are presented in Figures 2(a) and 2(b), respectively. In the para-equilibrium diagram, metastable phase boundary extensions when considering only the ferrite and austenite phases are shown in addition to phase equilibria when the liquid phase is included. In Figure 2(a), a vertical section of the ortho-equilibrium phase diagram is shown as a function of chromium content. Since a ternary Fe-Cr-Ni alloy is considered for ortho-equilibrium conditions, it must be remembered that tie-lines within the two phase region do not lie within the plane of the diagram. In Figure 2(b), the phase equilibria as a function of carbon content is displayed under para-equilibrium conditions. Since the relative amounts of Fe, Cr, and Ni are fixed under such para-equilibrium constraints, the phase diagram reduces to a "binary" diagram between (Fe,Cr,Ni) and C and the phase boundaries shown in Figure 2(b) also identify the tie-line compositions in the two-phase fields [20].

Ortho-Equilibrium Interface Condition

Simulations were carried out for isothermal annealing of an initially 100% ferrite structure at 1675,

1650, and 1630 K. These three temperatures were chosen for the following reasons: 1675 K is roughly the temperature at which ferrite solidification was completed, as concluded by Koseki [13], 1630 K is the temperature at which continuous cooling is interrupted, presumably due to austenite formation (see Figure 1(a)), and 1650 K is an intermediate temperature between these two limits. The simulation time was set to 200 s. The most rapid transformation rates were found for the isothermal simulation temperature of 1630 K. This is in spite of the fact that the diffusion coefficients are smaller at the lower temperature. The explanation is that as the temperature decreases, the product austenite composition is closer to the initial ferrite composition and the composition gradient within the ferrite, near the interface, becomes steeper. This combination leads to less solute buildup and higher fluxes, resulting in a faster transformation rate. Representative composition distributions for Cr and Ni at selected annealing times at 1630 K are shown in Figure 3. It can be seen that the austenite has grown only ~5 μm in 1 s at 1630 K. After 50 s, the austenite size has grown to ~45 μm. For all three annealing temperatures, the austenite product phase is basically uniform in composition. Only a very slight compositional gradient is present in the austenite at the start of the transformation and this is homogenized within approximately 0.1 s.

Calculations for the ortho-equilibrium condition with continuous cooling at 100 K/s from 1675 to 1475 K were also performed. A representative composition profile is shown in Figure 4. Under these conditions, the product austenite phase has a non-uniform composition; the austenite composition shows an increase of 1.7% Cr and decrease of 2% Ni (both absolute wt %) across its length. The austenite growth rate is rather limited as well, with only ~9 μm of austenite formed after cooling to 1475 K. If the simulations were continued below 1475 K, the calculations soon became unstable. This occurred as the chromium concentration of the austenite at the interface exceeded the chromium concentration in the ferrite far from the interface. Simultaneously, the austenite nickel concentration decreased below the ferrite nickel level. These conditions led to an escalating growth rate until an instability was reached.

One additional thermal history was examined for the ortho-equilibrium interface condition. The calculation cell was cooled from 1675 to 1630 K at 100 K/s, held at 1630 K for 0.5 s, and then cooled once again at 100 K/s to 1475 K. This thermal history is comparable to the experimentally measured thermal history shown in Figure 1(a) except that the hold at 1630 K is somewhat longer than the measured plateau of only 0.25 s. This thermal history did not produce any new results; the results were comparable to the continuous cooling results without an intermediate hold at 1630 K. The hold at 1630 K did not remove the composition gradient in the austenite and it did not yield any significantly greater amount of austenite formed.

Para-Equilibrium Interface Condition

In order to impose a para-equilibrium condition at the ferrite-austenite interface, the transformation must take place at a temperature within the two-phase (ferrite + austenite) phase field shown in the phase diagram in Figure 2(b) since the software did not allow for kinetic undercooling at the interface. This imposes a severe restriction on the allowed transformation temperatures. As can be seen in Figure 2(b), for an initial carbon concentration of 0.003 wt %, austenite formation can only begin at ~1714 K. Furthermore, the transformation cannot proceed below ~1710.5 K since two-phase para-equilibrium between ferrite and austenite does not exist below this temperature. Simulations were carried out under continuous cooling conditions from 1713 K. Numerical complications imposed some limitations on the cell sizes and cooling rate combinations that could be evaluated. Representative simulation results for the case of cooling at 50 K/s are shown in Figure 5, where the

composition is shown as a function of distance. By definition, the solute contents must be uniform across the ferrite-austenite interface if para-equilibrium exists, and Figure 5 confirms that this was the case in the simulation. A gradient in carbon concentration was found, as shown in Figure 5.

The austenite size as a function of time is shown in Figure 6. It is clear that the austenite growth rate is quite high; the austenite grows to 30 μm within 0.03 s (within 1.5 K). The austenite growth rate under ortho-equilibrium conditions is also shown in Fig 6 for comparison. In both calculations, the cooling rate was 50 K/s but the start temperatures for the two simulations were different. The ortho-equilibrium simulation was started at 1675 K while the para-equilibrium simulation was initiated at 1713 K. Figure 6 shows that transformation rates under para-equilibrium conditions are approximately two orders of magnitude greater than the rates under ortho-equilibrium conditions.

Discussion

In the simulations that were considered, either ortho-equilibrium or para-equilibrium conditions at the moving interface were imposed. The results of these calculations do not agree with the experimental measurements of Koseki and lead to the conclusion that neither interface condition is correct. In the case of ortho-equilibrium at the interface, uniform composition profiles in the product austenite phase could only be achieved for an isothermal simulation. However, the transformation rate was far too slow in the simulation. Whereas the experimental thermal profiles indicated the transformation was completed within approximately 0.25 s at 1630 K, the simulation indicated that less than 5 μm of austenite would form within this time. The size of the computational cell that is used will influence the transformation rate in that it will determine how soon impingement of the compositional profiles takes place. In addition, the cell size will directly control the percentage of the microstructure that corresponds to the 5 μm (or less) of transformed austenite. Examination of the microstructures showed that the grain size of the final austenite was on the order of 200 μm so the choice of a 100 μm cell size (half-width of the grain size) was quite reasonable. Even if the cell size were reduced to half this value, less than 10% of the ferrite would have been transformed within 0.25 s, indicating that the transformation rate in the ortho-equilibrium simulation is much too slow. Although somewhat more austenite is formed in the continuous cooling simulation, the transformation rate was still too slow and the resultant inhomogeneous composition profiles in the austenite disagree with the observed uniform austenite compositions.

Similarly, for the case of the simulations under para-equilibrium conditions at the interface, the simulation results did not agree with the experimental observations. Although the transformation rate under para-equilibrium conditions was considerably faster, and comparable to the transformation rates found experimentally, the para-equilibrium simulation could only take place at very high temperatures (~1710 K), much higher than the temperature at which the transformation was found to take place experimentally (~1630 K). This limitation is a consequence of the fact that there is no allowance for interface kinetics effects in the para-equilibrium calculations. Such kinetics effects could suppress the reaction temperature into the equilibrium single-phase region. The simulation under para-equilibrium conditions also produced a carbon gradient in the product austenite phase but this does not conflict with the experimental observations. First, during subsequent cooling, it is likely that the carbon gradient found in the simulations would be homogenized.

Second, carbon concentrations were not measured experimentally so no conflict with the experimental data exists.

There are, in theory, other simulations of the ferrite-to-austenite transformation that are possible and still are controlled by "local equilibrium" at the interface. The ortho- and para-equilibrium conditions represent limiting cases where substitutional solute diffusion is either complete or totally absent, respectively. It is certainly possible that some limited substitutional solute partitioning at the interface, in between the two limits of equilibrium partitioning (ortho-equilibrium) and no partitioning (para-equilibrium), takes place. Such a limited partitioning condition could eliminate many of the discrepancies that were found for the two simulations considered. The advantages of employing a limited solute partitioning condition at the interface can be identified by referring to a schematic phase diagram where hypothetical non-equilibrium phase boundaries are included. For discussion, a schematic phase diagram based on the ortho-equilibrium diagram in Fig. 2(a) is shown in Figure 7. The ortho-equilibrium phase boundaries between BCC (ferrite) and FCC (austenite) are shown as solid lines whereas the non-equilibrium boundaries that would result in non-equilibrium partitioning, and would correspond to conditions at some high growth velocity, are shown as dashed lines. For a composition C_0, the ortho-equilibrium transformation from BCC to FCC would begin at the BCC-solvus temperature T_1. For the product phase to have the same composition as the bulk parent phase under ortho-equilibrium conditions, the transformation would have to take place at the FCC-solvus temperature T_2. If the growth rate velocity was high, then only limited partitioning would take place and the non-equilibrium phase boundaries under these conditions, shown schematically by the dashed lines, would apply. Under these conditions, the product FCC phase would have the same composition of the overall alloy C_0 if the transformation took place at non-equilibrium FCC-solvus temperature T_3.

Applying these ideas to the present Fe-Cr-Ni-C alloy, one can make the following observations. Under ortho-equilibrium conditions, the simulation at 1630 K, corresponding to the observed transformation temperature, resulted in a transformation rate that was too slow. If the transformation were to take place at a lower temperature (the austenite solvus temperature), where the product austenite phase is of the same composition as the bulk alloy (temperature T_2 in Figure 7), then the transformation rate would likely be faster since the need for long range diffusion would be eliminated. However, for the Fe-Cr-Ni-C alloy under consideration, this austenite-solvus temperature is 1563 K, which is far below the experimentally observed transformation temperature. On the other hand, under para-equilibrium conditions, the austenite-solvus is around 1710 K, far above the experimentally observed transformation temperature. The actual transformation temperature, ~1630 K, was between these two limits. If only limited partitioning of substitutional solutes occurred, then the austenite-solvus under these non-equilibrium conditions would be between these two extremes. At a sufficiently high velocity, the non-equilibrium solvus temperature could increase to the neighborhood of 1630 K. This is still well below the upper bound for the austenite-solvus, which is the T_0 temperature, and was calculated to be 1713.5 K for the Fe-Cr-Ni-C alloy under consideration. Under the conditions of limited solute partitioning, an isothermal planar growth transformation would lead to a product phase of exactly the same composition as the overall bulk composition. In addition, with no change in bulk parent and product compositions, the transformation rate would be considerably greater than that found for the ortho-equilibrium simulation. Thus, a local equilibrium condition with some, non-zero, limited substitutional solute partitioning could provide the necessary conditions to reproduce the experimental observations.

The problem in the implementation of a limited partitioning condition lies with the inability to describe the limited partitioning behavior for a multi-component system. Such a description is not currently available in the computational thermodynamic models or in the multi-component kinetic models such as the Dictra and MatCalc codes used in this work. Unfortunately, only the two extremes of ortho- and para-equilibrium conditions at the interface can be examined at present. If and when such non-equilibrium partitioning can be implemented in these codes, it is possible that all the features of the experimental results could be simulated properly and, thereby, explained.

Summary and Conclusions

The ferrite to austenite transformation was modeled by assuming a diffusion-controlled transformation reaction and by considering two different conditions at the transformation interface. The first condition specified ortho-equilibrium at the interface and allowed for long-range diffusion of substitutional solute elements. The second condition imposed para-equilibrium at the interface, thereby limiting long-range diffusion to interstitial alloying elements only (carbon). Neither interface condition could reproduce the experimental results. The ortho-equilibrium condition yielded transformation rates that were far too slow compared to the experimental measurements of Koseki. Although the para-equilibrium interface condition yielded transformation rates that were comparable to the experimental results, the transformation temperature necessary for this condition was considerably higher than that found experimentally. It is concluded that an intermediate interface condition could yield results in much better agreement with the experimental findings. Such a condition would involve limited partitioning of substitutional solute elements. However, implementation of this condition is not possible at present because it cannot be included in the kinetic models that are currently available.

Acknowledgments

This research was sponsored by the Division of Materials Sciences and Engineering, U. S. Department of Energy, under contract DE-AC05-00OR22725 with UT-Battelle, LLC.

References

1. S. A. David, J. M. Vitek, and T. L. Hebble, *Weld. J.*, **66** (1987) 289s-300s.
2. S. Katayama and A. Matsunawa, *Proceedings of the International Conference on Applications of Lasers and Electro-Optics*, Laser Institute of America, 1985, 19-25.
3. Y. Nakao, K. Nishimoto, and W. P. Zhang, *in Proceedings 4th International Colloquium on Welding and Melting by Electron and Laser Beams*, eds. M. Contré and M. Kuncevic, French Institute of Welding, 1988, 673-680.
4. J. W. Elmer, S. M. Allen, and T. W. Eagar, *Metall. Trans. A*, **20A** (1989) 2117-2131.
5. For more detailed review, see J. M. Vitek and S. A. David, in *Laser Materials Processing - IV*, eds. J.

Mazumder, K. Mukerjee and B. L. Mordike, TMS-AIME, Warrendale, PA,1994, 153-167.

6. T. F. Kelly, M. Cohen, and J. B. VanderSande, *Metall. Trans. A*, **15A** (1984) 819-833.
7. M. Bobadilla, J. Lacaze, and G. Lesoult, *J. Cryst. Growth*, **89** (1988) 531-544.
8. W. Löser and D. M. Herlach, *Metall. Trans. A*, **23A** (1992) 1585-1591.
9. T. Koseki and M. C. Flemings, *Metall. Mater. Trans. A*, **27A** (1996) 3226-3240.
10. S. Fukumoto and W. Kurz, *ISIJ Int.*, **39** (1999) 1270-1279.
11. J. Singh, G. R. Purdy, and G. C. Weatherly, *Metall. Trans. A*, **16A** (1985) 1363-1369.
12. J. A. Brooks, M. I. Baskes, and F. A. Greulich, *Metall. Trans. A*, **22A** (1991) 915-926.
13. T. Koseki, PhD Thesis, Massachusetts Institute of Technology, Cambridge, MA, 1994.
14. T. Koseki, Nippon Steel Corporation, Futtsu, Japan, personal communication, 2001.
15. J.-O. Andersson, L. Hoglund, B. Jonsson, and J. Ågren, in *Fundamentals and Applications of Ternary Diffusion*, ed. G. R. Purdy, Pergamon Press, New York, 1990, 153-163.
16. B. Sundman, B. Jonsson, and J.-O. Andersson, *Calphad*, **9** (1985) 153-190.
17. B. Sundman, SGTE Solution Database, Royal Institute of Technology, Stockholm, Sweden, 1992.
18. E. Kozeschnik, Dr-Ing Thesis, Graz University of Technology, Graz, Austria, 1997.
19. E. Kozeschnik, *Calphad*, **24** (2001) 245-252.
20. E. Kozeschnik, *J. Phase Equil.*, **21** (2000) 336-341.

a)

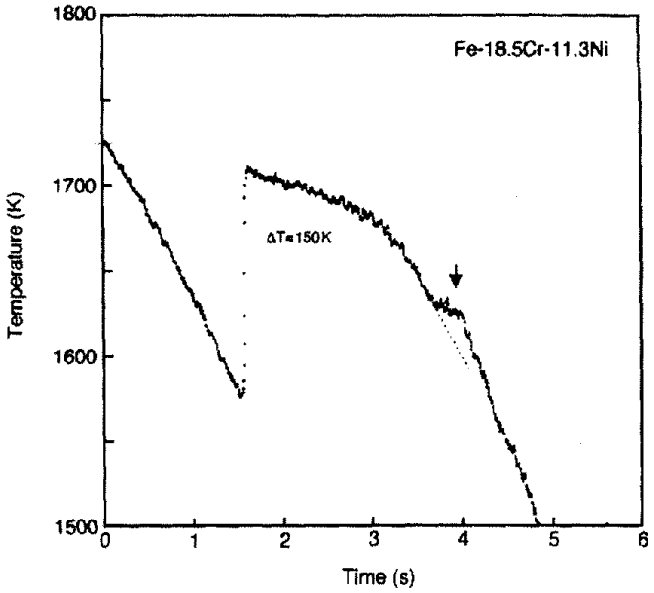

b)

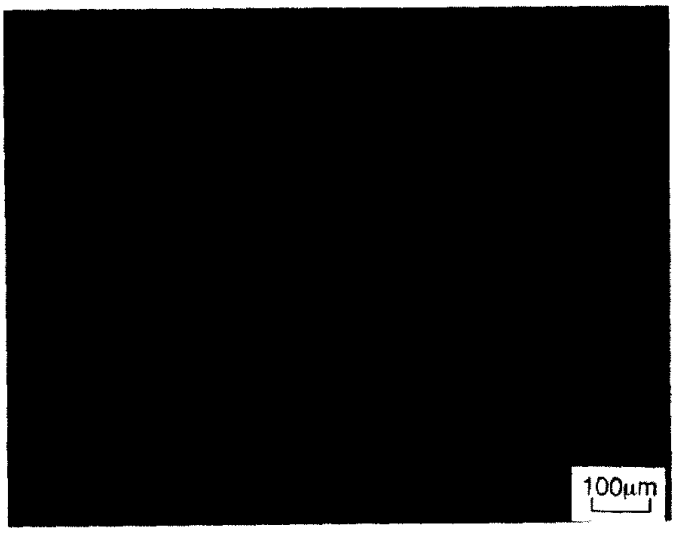

Fig. 1 (a) thermal profile of highly undercooled droplet that was 100% austenite (near the surface) and showed characteristics of a massive ferrite to austenite transformation. (b) corresponding micrograph showing completely austenitic microstructure near the surface and no signs of dendritic solidification substructure (taken from ref. 13).

a)

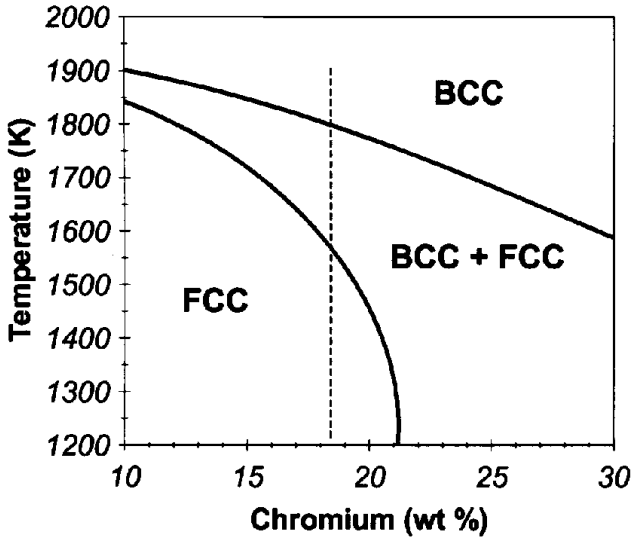

b)

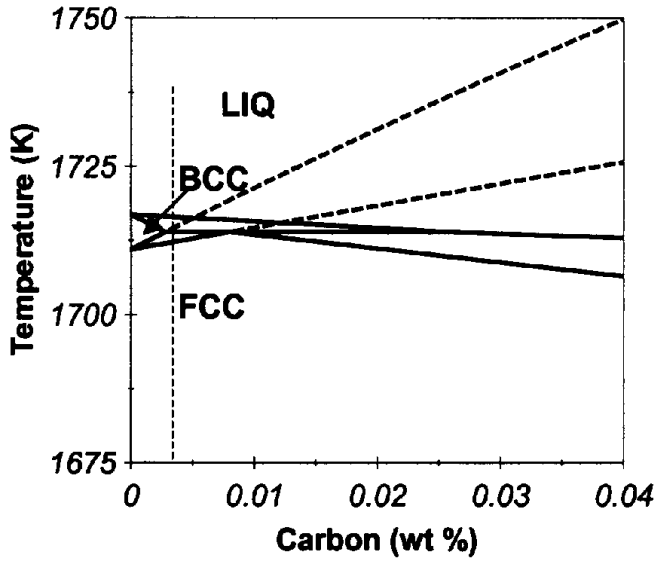

Fig. 2 (a) vertical section of ortho-equilibrium phase diagram for Fe-Cr-Ni at 11.34 wt % Ni showing the ferrite (BCC) and austenite (FCC) phase fields and (b) para-equilibrium phase diagram for Fe-18.51Cr-11.34Ni-C showing equilibrium liquid, ferrite (BCC) and austenite (FCC) phase fields as well as metastable extensions of BCC-FCC equilibrium. Diagrams were calculated using the MatCalc program [18]. Alloy composition considered in this investigation is shown by vertical dashed line.

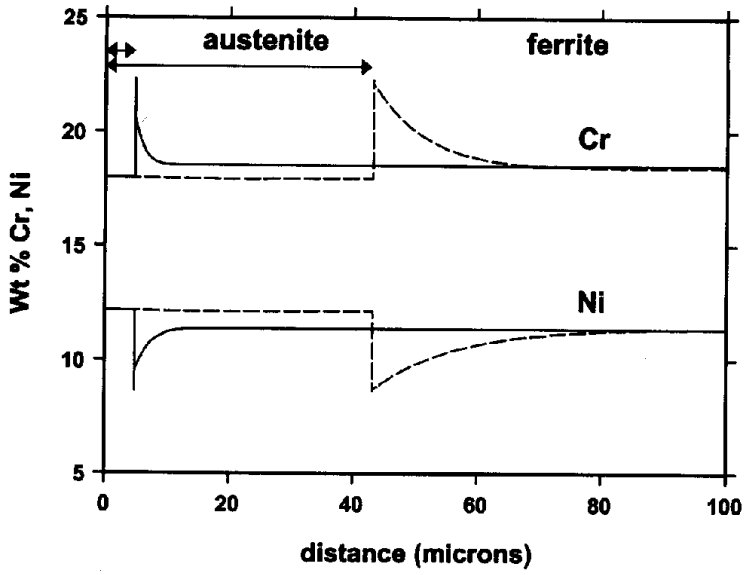

Fig. 3 Composition profiles for isothermal (1630 K) simulation with ortho-equilibrium at the interface. The solid lines are after 1 s at 1630 K; the dashed lines are for 50 s at 1630.

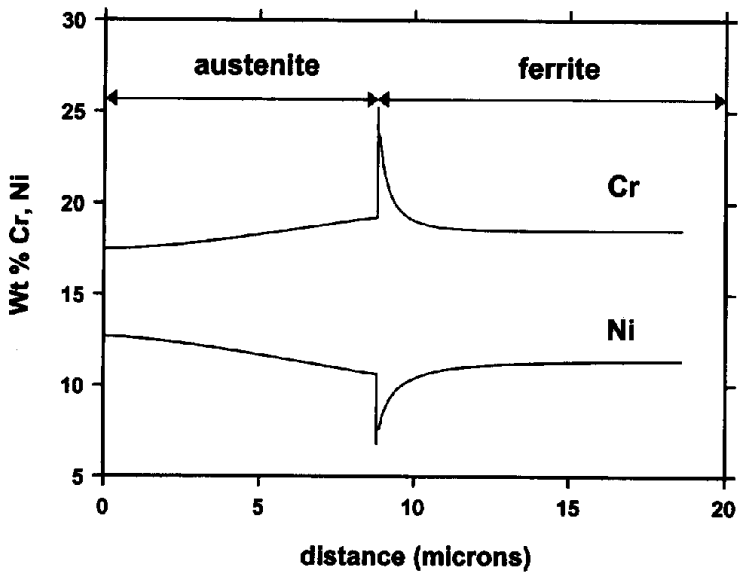

Fig. 4 Composition profiles for simulation with ortho-equilibrium at the interface after continuous cooling (100 K/s) from 1675 to 1475 K.

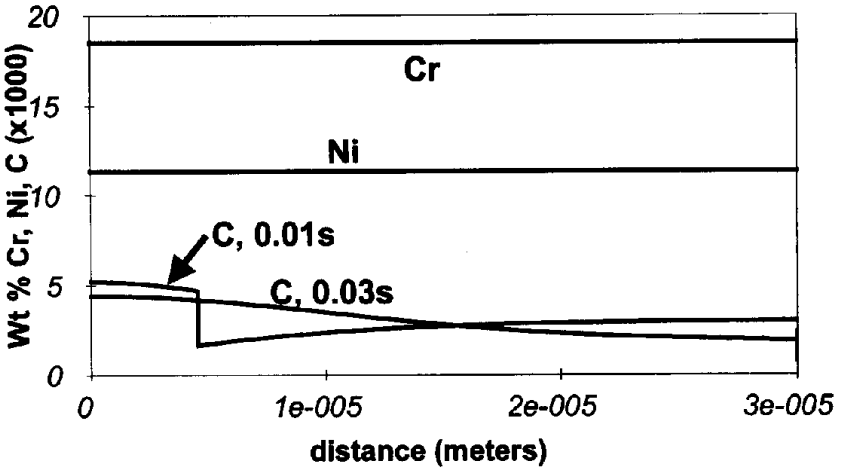

Fig. 5 Composition profiles for simulation with para-equilibrium at the interface after continuous cooling at 50 K/s from 1713 K (T = 1712.5 K after 0.01 s and 1711.5 K after 0.03 s). A carbon gradient is revealed, but the chromium and nickel profiles are uniform, which is required by definition for para-equilibrium conditions.

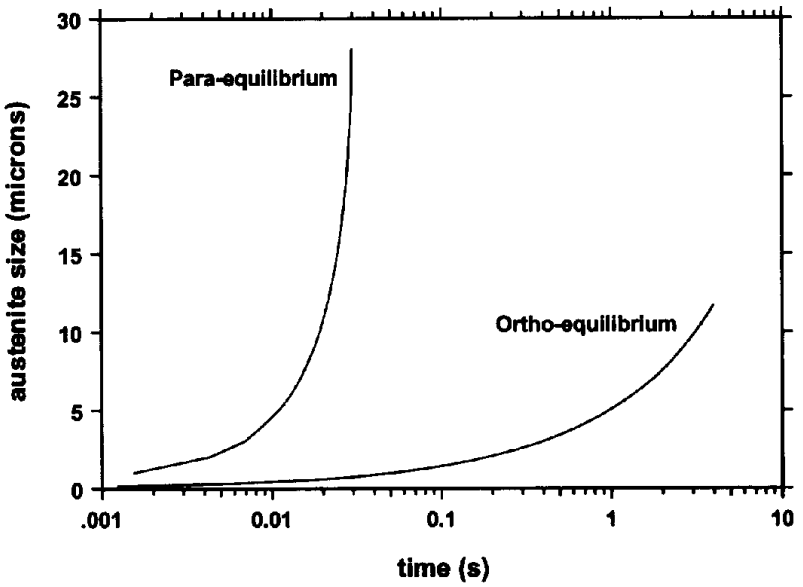

Fig 6 Austenite size as a function of time during cooling at 50 K/s under para-equilibrium conditions at the interface. Comparable plot for cooling under ortho-equilibrium conditions at the interface is also plotted. Note that cooling under para-equilibrium conditions is from 1713 K while cooling for ortho-equilibrium conditions is from 1675 K.

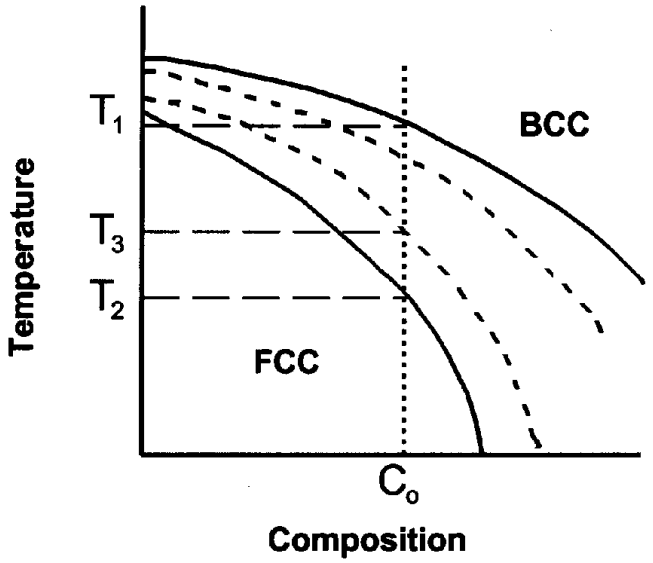

Fig 7 Schematic diagram based on ortho-equilibrium phase diagram section shown in Fig 2(a) showing equilibrium phase boundaries (solid lines) and non-equilibrium phase boundaries (dashed lines) under conditions of high growth velocity with limited solute partitioning. Meaning of various temperatures is described in text.